

Are Compact High-Velocity Clouds Extragalactic Objects?

Philip R. Maloney¹ & Mary E. Putman^{2,3}

*Center for Astrophysics and Space Astronomy, University of Colorado
Boulder, CO 80309-0389*

ABSTRACT

Compact high-velocity clouds (CHVCs) are the most distant of the HVCs in the Local Group model and, at $d \sim 1$ Mpc, they have HI volume densities of $\sim 3 \times 10^{-4} \text{ cm}^{-3}$. Clouds with these volume densities and the observed column densities $N_{\text{HI}} \sim 10^{19} \text{ cm}^{-2}$ will be largely ionized, even if exposed only to the extragalactic ionizing radiation field. Here we examine the implications of this process for models of CHVCs. We have modeled the ionization structure of spherical clouds (with and without dark matter halos) for a large range of densities and sizes, appropriate to CHVCs over the range of suggested distances, exposed to an extragalactic ionizing photon flux $\phi_i \sim 10^4 \text{ phot cm}^{-2} \text{ s}^{-1}$. Constant-density cloud models in which the CHVCs are at Local Group distances have total (ionized plus neutral) gas masses $\sim 20 - 30$ times larger than the neutral gas masses, implying that the gas mass alone of the observed population of CHVCs is $\sim 4 \times 10^{10} M_{\odot}$. With a realistic (10:1) dark matter to gas mass ratio, the total mass in such CHVCs is a significant fraction of the dynamical mass of the Local Group, and their line widths would greatly exceed the observed ΔV . Self-consistent models of gas in dark matter halos fare even more poorly; they must lie within approximately 200 kpc of the Galaxy, and (for a given distance) are much more massive than the corresponding uniform density models. We also show that exponential neutral hydrogen column density profiles are a natural consequence of an external source of ionizing photons, and argue that these profiles cannot be used to derive model-independent distances to the CHVCs. These results argue strongly that the CHVCs are not cosmological objects, and are instead associated with the Galactic halo.

Subject headings: ISM: clouds — ISM: H I — Galaxy: halo — Local Group

1. Introduction

The anomalous velocity clouds of neutral hydrogen known as the high-velocity clouds (HVCs) may represent the continuing infall of matter onto the Local Group (*e.g.*, Oort 1966; Verschuur 1969; Blitz *et al.* 1999). The distances to the majority of these clouds remains unknown, but in the

¹maloney@casa.colorado.edu

²Hubble Fellow

³mputman@casa.colorado.edu

Local Group scenario the distances would range from a few kpc (for gas currently accreting onto the Galaxy) to beyond Andromeda (~ 1 Mpc). HVCs range in size from $\sim 0.1 - 100$ deg², and it is possible that the sizes reflect their distance from the Galaxy. In particular, some of the HVCs are both compact and isolated from extended emission, and show many similar HI properties to dwarf galaxies. These are referred to as compact HVCs (CHVCs) and may be the pristine building blocks of the Local Group at ~ 1 Mpc.

The survival and composition of these CHVCs against photoionization depends on their volume densities (and therefore distances) and the strength of the extragalactic ionizing photon flux. The presence of an extragalactic ionizing radiation field is inferred from several sets of observations. Maloney (1993) used a deep H I observation of NGC 3198 (van Gorkom 1993), which shows a sharply truncated neutral hydrogen disk at $N_{\text{HI}} \approx 5 \times 10^{19}$ cm⁻², to infer that the flux in the energy range $h\nu = 13.6$ to ~ 200 eV is approximately $\phi_i = 10^4$ phot cm⁻² s⁻¹. Estimates from the proximity effect at low redshift (Kulkarni & Fall 1993; Scott *et al.* 2002), upper limits from sensitive H α observations (Madsen *et al.* 2001; Weymann *et al.* 2001), and theoretical estimates based on known sources (Haardt & Madau 1996; Shull *et al.* 1999) are in agreement with a value $\phi_i \sim 0.5 - 1.5 \times 10^4$ phot cm⁻² s⁻¹.

In this paper we examine the ionization state of the compact high-velocity clouds at various distances, subject to an extragalactic ionizing radiation field. In the original Local Group model, the CHVCs are confined by dark matter halos, with $M_{\text{dm}}/M_{\text{gas}} \approx 10$. In a more recent variant of this model, it is suggested that the CHVCs are condensations in an intragroup medium, bound by external pressure (Blitz, private communication). We therefore consider both constant gas density models and dark matter-dominated models. The H I properties of the CHVCs are briefly reviewed in section 2 and the photoionization model is described in section 3. The results of the models are presented in section 4, and in section 5 we discuss the implications of the results.

2. HI Data

The H I properties of the CHVCs are taken from the H I Parkes All-Sky Survey (HIPASS) HVC catalog of Putman *et al.* (2002). This is a catalog of high-velocity clouds with declination $\delta < +2^\circ$ and $|v_{\text{LSR}}| \leq 500$ km s⁻¹, excluding emission with $|v_{\text{LSR}}| < 90$ km s⁻¹ to avoid confusion with Galactic emission. The spatial resolution of the survey is $15.5'$ and the velocity resolution is 26 km s⁻¹. The 5σ column density sensitivity of the HVC HIPASS data is 2×10^{18} cm⁻², which we adopt as a cutoff. Barnes *et al.* (2001) give a full description of HIPASS. The original CHVC catalog of Braun & Burton (1999) was based on data of lower resolution and sensitivity, and 50% of the CHVCs in the region of overlap between the two catalogs were reclassified based on the HIPASS data. In order for a high-velocity cloud to be considered a compact and isolated CHVC in the HIPASS catalog, it must have a diameter at 25% of the peak column density less than 2° , and must not be elongated in the direction of any extended emission. The typical parameters of a HIPASS CHVC are an angular size of 0.36 deg² (to the sensitivity limit), a total H I flux of 19.9 Jy km s⁻¹, and a typical peak column density of $N_{\text{HI}} \sim 10^{19}$ cm⁻². There are a total of 179

CHVCs cataloged from HIPASS and when this is combined with the northern sky data from the Leiden-Dwingeloo survey there are approximately 250 CHVCs in total (de Heij, Braun & Burton 2002). The linewidth distribution shows a prominent peak at a FWHM $\Delta V = 25 \text{ km s}^{-1}$ (de Heij, Braun & Burton).

For most of the results in this paper, we have used the typical CHVC parameters quoted above. This is a reasonable assumption, since the distributions in column density, angular size, and velocity are fairly sharply peaked. An increase or decrease of less than a factor of three in column density away from the peak value produces a drop by a factor of five or more in the number of clouds⁴, and similarly for the cloud areas (*cf.* Figures 12 and 13 of Putman *et al.* [2002]). The linewidth distribution of de Heij *et al.* (2002) is less sharply peaked than the column density or angular size distributions, and is skewed to the low-velocity end: 70% of the observed clouds have a FWHM $\Delta V = 25 \text{ km s}^{-1}$ or less; less than 10% have ΔV in excess of 42 km s^{-1} . Despite the well-defined typical values, in order to verify that our conclusions are robust to uncertainties in the cloud parameters, we have also included models in which the peak central column density is up to an order of magnitude larger than the typical CHVC value, and the linewidth is doubled to $\Delta V = 50 \text{ km s}^{-1}$ (see §4.2.2).

3. Model

The photoionization models of CHVCs have been calculated with the code described by Maloney (1993), modified to allow for the spherical geometry of the CHVCs. (Modest – tens of percent – departures from sphericity will have no significant impact on the model results.) Spherical geometry raises the ionization rates substantially over plane-parallel models with the same total hydrogen density; integration of the ionization rates over angle is done using 10-point Gaussian quadrature. The photoionization equilibrium of a CHVC exposed to an isotropic background radiation field is calculated iteratively, including the effects of the diffuse radiation. Thermal equilibrium at $T \sim 10^4 \text{ K}$ is assumed, as is appropriate for gas in the warm neutral phase. An ionizing photon flux $\phi_i \approx 10^4 \text{ phot cm}^{-2} \text{ s}^{-1}$ has been assumed; a flux a factor of two smaller would reduce the total gas masses by a factor of ≈ 1.5 (see below). A radial grid with 100 depth points (with logarithmic spacing) was used; we have verified that this provides adequate accuracy (less than 1% error in the total column density for a fixed neutral column density). In all cases we have assumed that the only ionizing photon flux is due to the extragalactic background; depending on the fraction of ionizing photons that escape from the Milky Way, the Galactic ionizing radiation field could dominate for CHVC distances $d \lesssim 100 \text{ kpc}$ (Maloney & Bland-Hawthorn 1999).

⁴Sensitivity starts to affect the column density distribution for column densities not too far below the peak, and so the drop-off with decreasing column below the peak is not reliably established. However, since clouds with column neutral hydrogen column densities smaller than the peak value will be even more highly ionized than clouds with our typical parameters, the actual number of clouds at the low column density end is irrelevant for the purposes of this paper.

4. Results

As noted in the introduction, we have considered both models with uniform gas (total hydrogen) density n_{H} and models where the gas is confined by dark matter potential wells. We first discuss the constant n_{H} models, as these contain much of the relevant physics, and then the models that include dark matter.

4.1. Uniform density models

If the CHVCs were at local group distances (~ 1 Mpc), their H I volume densities would be $n_{\text{HI}} \sim 10^{-4} \text{ cm}^{-3}$. We therefore consider total hydrogen densities n_{H} ranging from 10^{-4} to 10^{-2} cm^{-3} ; as we will see, the low-density end of this range is untenable for reasonable HVC distances. The model results (total hydrogen columns, gas masses, etc.) are given in Table 1.

In Figure 1, we plot the column density of total hydrogen that is required to produce a neutral hydrogen column $N_{\text{HI}} = 10^{19} \text{ cm}^{-2}$ as a function of the total hydrogen density, when the model CHVCs are exposed to our fiducial ionizing photon flux. The solid curve is for our fiducial ionizing photon flux and the dashed curve is for ϕ_i reduced by a factor of two. At the low density end of the range, the ratio $N_{\text{H}}/N_{\text{HI}}$ is enormous, $\sim 100 - 200$, in consequence of the small neutral fraction of gas at this density even if exposed only to the extragalactic ionizing background. At the highest densities, this ratio has declined to $\approx 2.5 - 3$, as the gas is substantially neutral over much of the total column.

Since we know both the neutral and total hydrogen column densities as well as the volume densities, we can calculate the gas masses directly from the models. However, in order to compare the results to observations, we need to assign distances to the model clouds. To do this, we adopt the following procedure. For each model, we determine the radius at which the projected H I column drops to the HIPASS sensitivity limit of $N_{\text{HI}} = 2 \times 10^{18} \text{ cm}^{-2}$. We then set the distance by requiring that the apparent angular size (using this radius) matches the typical value found for the CHVCs in the HIPASS survey, for which the angular radius $\Delta\theta \sim 0.34$ degrees. This gives the result $d_{\text{HVC}} = 169R_{18.3}$ kpc, where $R_{18.3}$ is the model radius (in kpc) at the $N_{\text{HI}} = 2 \times 10^{18} \text{ cm}^{-2}$ level.

In Figure 2 we show both the total gas masses M_{gas} and the apparent masses M_{HI} , the latter derived from the neutral hydrogen column densities and the apparent (as measured in H I) sizes, as a function of the cloud distance and total gas volume density, for our fiducial ionizing photon flux. As is evident from Table 1, models in which the total gas density is less than $n_{\text{H}} \sim 3 \times 10^{-3}$ are ruled out, as such clouds are so large that they are required to lie outside of the Local Group, and the gas masses become absurdly large. At the maximum acceptable distance ($d \sim 1$ Mpc) the total gas mass is an order of magnitude larger than the apparent H I mass.

Figure 3 shows the same quantities as in Figure 2, but we now show the results only for clouds within the Local Group ($d \leq 1$ Mpc). In addition, this figure also shows the gas masses for ϕ_i a factor of two smaller than our assumed value. For the lower photon flux, clouds of a fixed density are at smaller radius compared to the fiducial model. At a fixed distance, the total gas masses are

smaller by about a factor of 1.5 for the reduced flux models. For model CHVCs at Local Group distances ($d \gtrsim 0.5$ Mpc), the gas masses are $M_{gas} \sim 10^7 - 10^8 M_{\odot}$.

There is an additional constraint that we can apply to the CHVC models. The linewidth distribution of CHVCs is sharply peaked at a FWHM $\Delta V \approx 25 \text{ km s}^{-1}$ (de Heij, Braun, & Burton 2002). We have therefore calculated the expected line FWHM for the models (*i.e.*, using the velocity dispersion for a self-gravitating system), both with and without a dark matter component (in the former case the total mass has simply been scaled up by the assumed ratio of dark to baryonic mass); ΔV has been calculated assuming a uniform spherical mass distribution. In Figure 4 we show the predicted line FWHM as a function of distance, for dark matter to gas mass ratios of ten and zero. In the former case, the models are consistent with the observations for a distance $d \sim 330$ kpc; with no dark matter the clouds must lie at approximately 1.5 Mpc. For ϕ_i reduced by a factor of two, these distances increase somewhat, to $d \sim 430$ kpc and 2.1 Mpc for $M_{dm}/M_{gas} = 10$ and no dark matter, respectively.

While these models rule out the possibility that the CHVCs sample a population of cosmological objects (*i.e.*, gas in dark matter-dominated potential wells) at distances characteristic of the Local Group ($d \sim 1$ Mpc), they suggest that they could represent such objects at distances of $\sim 300 - 400$ kpc. However, as we will see in the next section, models of CHVCs in realistic dark matter potential wells require that they lie much closer to the Galaxy, with an upper limit to the distance of about 200 kpc. This distance scale rules out models in which the CHVCs represent continuing infall onto the Local Group.

4.2. Dark matter halo models

Motivated by the order-of-magnitude agreement between the properties of model clouds with $M_{dm}/M_{gas} \sim 10$ and the observations for characteristic distances $d \sim 350$ kpc, we have constructed models of CHVCs using realistic dark matter potential wells. Numerical simulations of halo formation in cold dark matter cosmologies predict a specific form for the density profile, as initially found by Navarro, Frenk, & White (1996). However, there is considerable disagreement as to whether this profile describes the halos of real galaxies, particularly dwarf and low-surface brightness galaxies (*e.g.*, Flores & Primack 1994; Moore 1994; Burkert 1995). A number of authors have argued that these latter objects have nearly constant-density cores rather than the cusped power-law NFW density profile, but this point is controversial. We have therefore adopted two different models for the halo profile. The first is the the Navarro, Frenk, & White (1996) halo density profile, but modified to allow for the possible presence of a density core:

$$\rho_{dm}(r) = \rho_{crit} \frac{\delta_c r_s}{(r + r_o)(1 + r/r_s)^2} \quad (1)$$

where $\rho_{crit} = 3H^2/8\pi G$ is the closure density, the scale length r_s is related to the virial radius of the halo by the concentration parameter $c = R_{vir}/r_s$, r_o is the core radius, and δ_c is a characteristic density contrast, determined by the requirement that the halo mass

$$M_h(R_{vir}) = \Delta \rho_{crit} (4\pi/3) R_{vir}^3, \quad (2)$$

where Δ is the overdensity parameter. For a flat ($\Omega + \Lambda = 1$) universe, Δ is given by (*e.g.*, Eke, Navarro, & Frenk 1998) $\Delta = 178\Omega^{0.45} \approx 111$ at $z = 0$ for the $\Omega_{dm} = 0.35$ cosmology adopted here. For the relevant mass range of halos, $c \sim 10$.

In the limit of no core, the density contrast is given by the standard result (*e.g.*, Eke, Navarro, & Steinmetz 2001)

$$\delta_c = \frac{\Delta}{3} \frac{c^3}{\ln(1+c) - c/(1+c)}. \quad (3)$$

Since we have no physical basis for choosing the core radius (this point is discussed further below) we have kept the concentration parameter fixed (for a given halo mass) at the no-core value, and calculated δ_c from the requirement that the integral of equation (1) to R_{vir} equal the mass given by equation (2). The NFW halo parameters (c , R_{vir}) for a given mass have been calculated using the results of Mo, Mao & White (1998) and Eke *et al.* (2001).

The second halo mass profile is that suggested by Burkert (1995) based on observations of dwarf galaxies,

$$\rho_{dm}(r) = \frac{\rho_o r_o^3}{(r + r_o)(r^2 + r_o^2)} \quad (4)$$

where ρ_o is the core density and r_o is again the core radius. Like the NFW profile, the density of the Burkert halo falls as r^{-3} at large radius. Burkert found that the core density and radius were tightly correlated for the observed galaxies, so that the dark matter profiles are described by only one free parameter, which can be taken to be r_o . Burkert also concluded that the halo virial radius $R_{vir} \approx 3.4r_o$, so that these halos are much less centrally concentrated than the NFW halos.

We have calculated the gas density profile within these halos, including the effects of the gas self-gravity. The dark matter density profile is fixed, however: we do not include the response of the halo to the gas. (This would only strengthen our conclusions on the viability of models with dark matter.) In most cases, the gas velocity dispersion is taken to be $\sigma_g = 10.6 \text{ km s}^{-1}$, which produces a line FWHM equal to the typical observed value $\Delta V = 25 \text{ km s}^{-1}$, and is the expected value for gas at $T \sim 10^4 \text{ K}$, characteristic of the warm neutral medium. For NFW halos, in the case of no core and negligible gas self-gravity, the gas density profile is given by

$$\rho_g(\tilde{r}) = \rho_g(0)e^{C_h[\ln(1+\tilde{r})/\tilde{r}-1]} \quad (5)$$

where $\tilde{r} = r/r_s$ and

$$C_h = \frac{4\pi G \rho_{crit} \delta_c r_s^2}{\sigma_g^2} = 7.34 \times 10^{-3} \frac{\delta_c r_s^2}{\sigma_g^2} \quad (6)$$

for r_s in kpc and σ_g in km s^{-1} . For Burkert halos the gas profile is not analytic even in the absence of self-gravity.

We first discuss the results of models with NFW halos, and then the Burkert halo models.

4.2.1. NFW halo models

The uniform density models that are consistent with a dark matter to baryon ratio of about 10 have total hydrogen volume densities of approximately $3 \times 10^{-3} \text{ cm}^{-3}$ and total gas masses of

about $M_{gas} \approx 1.4 \times 10^7 M_{\odot}$. We have therefore calculated the gas distribution and the neutral fraction for a halo with a mass $M_{dm} = 1.4 \times 10^8 M_{\odot}$. The virial radius of this halo is 13 kpc and the concentration parameter $c = 12.44$. We have also allowed for tidal truncation of the halo due to the Galaxy’s tidal field; this introduces a cutoff at a radius of 10.2 kpc.

In Figure 5 we show the gas density profile for the model that satisfies the requirement that the peak $N_{\text{HI}} = 10^{19} \text{ cm}^{-2}$. This profile (which is characteristic of all the halo models) immediately reveals the problem that plagues all of these models. Most of the gas mass in the halo is at large radius, where the density is low and therefore the neutral fraction is very small. Hence, in order to match the observed neutral column density, the density at the center of the halo must be raised substantially over that in the uniform density model. As Figure 6 (which plots the cumulative dark matter and gas masses as a function of radius) demonstrates, this large central gas density results in a gas to dark matter mass ratio of approximately unity within the halo, which is obviously untenable. This conclusion is unaltered by reducing the ionizing flux by a factor of two or by allowing the dark matter profile to have a core. Although this latter modification results in gas density profiles that are more nearly constant over a larger range in radius, and therefore produce the same total hydrogen column density for a smaller central density, the slower drop-off of n_{H} with r due to the core means that these models always have a higher value of M_{gas}/M_{dm} at the outer boundary than the no-core models. (In fact, the models with cores invariably require larger total hydrogen columns than the models without cores, which makes the problem even worse.)

The only way to produce reasonable baryon to dark matter ratios in these models is to increase the mass of the halo. In order to produce a model in which the ratio M_{gas}/M_{dm} is less than about 0.1^5 at the outer boundary *prior* to tidal truncation, the halo mass must be $M_{dm} \gtrsim 5 \times 10^8 M_{\odot}$. The mass increase is smaller than the factor of ten one might expect from Figure 6 because higher mass halos are both larger than lower mass ones and denser at the same physical radius, and therefore the observed neutral hydrogen column can be produced with a smaller total gas mass than is required in the lower mass halo.

In addition to the mass problem, to which we return below, these NFW dark matter-dominated models suffer from another, severe problem for the cosmological hypothesis: the physical size of the neutral hydrogen distribution is so small that the model CHVCs are restricted to lie less than $d \sim 200$ kpc from the Galaxy. This is illustrated in Figure 7, which shows the projected H I column as a function of impact parameter for a variety of halo masses, core radii, and ionizing fluxes. *In no case does the model CHVC radius at the HIPASS threshold, $R_{18.3}$, significantly exceed 1 kpc.* As discussed in §4.1, this constrains the clouds to distances of no more than about 200 kpc from the Galaxy. In fact, except for the lowest mass ($M_{dm} = 1.4 \times 10^8 M_{\odot}$) model shown in Figure 7, which, as discussed above, has an unacceptably large gas to dark matter mass ratio, all of the models have $R_{18.3} \lesssim 0.5$ kpc unless we include a core in the halo density distribution. As we noted earlier, we have no physical basis for choosing the halo core parameters, and have included a core simply to

⁵Assuming that galaxy clusters provide a fair sample of the universe, the baryon to dark matter mass ratio is estimated to be 0.13 for $H_o = 70 \text{ km s}^{-1} \text{ Mpc}^{-1}$ (Mohr, Mathiesen, & Evrard 1999).

see whether, given the uncertainties in the actual halo dark matter profiles, this could alleviate the problems arising from the small distance scale mandated by the small physical size of the model CHVCs. As is evident from Figure 7, it does not. The reason is simply that if the halo is massive enough that the observed neutral hydrogen column density can be reproduced with a reasonable baryon to dark matter mass ratio, the velocity dispersion of the baryonic component (which is fixed by the observed linewidth) is only a fraction of the velocity dispersion characterizing the dark matter potential well, with the result that the gas is confined to the core of the halo. Increasing the size of the core beyond $r_o \approx r_s$ does not lead to any significant further increase in $R_{18.3}$, as is seen in the right-hand panel of Figure 7.

4.2.2. Burkert halo models

In Figure 8 we show results for models with a Burkert halo of mass $M_{dm} = 10^8 M_\odot$. For these models we have also explored a larger region of parameters for the CHVCs, considering neutral hydrogen columns up to ten times larger than the typical value seen in the HIPASS survey and linewidths up to a factor of two larger than the typical value. The left-hand panel assumes the standard velocity dispersion of $\sigma_g = 10.6 \text{ km s}^{-1}$. From left to right, we plot the neutral hydrogen column as a function of impact parameter for peak neutral hydrogen column densities $N_{\text{HI}} = 10^{19} \text{ cm}^{-2}$ (solid line), $N_{\text{HI}} = 2.5 \times 10^{19} \text{ cm}^{-2}$ (long-dashed line), $N_{\text{HI}} = 5.0 \times 10^{19} \text{ cm}^{-2}$ (dotted line), $N_{\text{HI}} = 7.5 \times 10^{19} \text{ cm}^{-2}$ (short-dashed line) and $N_{\text{HI}} = 10^{20} \text{ cm}^{-2}$ (solid line). This Burkert halo model does not suffer from the unacceptably high baryon to dark matter mass ratio problem that afflicts the NFW halos of comparable mass, because the Burkert halo is physically much smaller (virial radius of 1.8 kpc compared to 11.7 kpc for the same mass NFW model) and therefore its mean density is much higher than the corresponding NFW halo. However, this small size scale becomes a serious problem just as it does for the NFW halos. Even for a peak column $N_{\text{HI}} = 10^{20} \text{ cm}^{-2}$, the projected size at the HIPASS sensitivity threshold barely reaches 1 kpc, again implying that the halos are no more than 200 kpc distant. The right-hand panel shows the same models, only for a doubled velocity dispersion, so that the line FWHM $\Delta V = 50 \text{ km s}^{-1}$. Even with this assumption, the physical size of the clouds remains small: raising the peak column density to $N_{\text{HI}} = 5.0 \times 10^{19}$ - five times the typical HIPASS value - only increases the cloud radius to about 1.6 kpc, which would push the clouds out to no more than 270 kpc. (Lower mass halos - *e.g.*, $10^7 M_\odot$ - with Burkert profiles are so small that they can lie no further than $d \sim 100$ kpc from the Milky Way, independent of total column density.)

In Figure 9 we present similar results, but for a halo with $M_{dm} = 10^9 M_\odot$. In the left-hand panel, with a velocity dispersion corresponding to the typical observed value, the results scarcely differ from those for the $10^8 M_\odot$ halo, and the cloud size at the HIPASS threshold again never exceeds 1 kpc. The results for the models with twice the linewidth are also very similar to those for the lower mass Burkert halo. The chief difference is that, since the $10^9 M_\odot$ halo is physically larger (by a factor of 2.7) than the $10^8 M_\odot$ halo, the highest column density models are larger in the higher mass model, since the column density cutoff is not set by the physical edge of the halo

as it is in the $10^8 M_\odot$ model.

Hence the CHVC models with Burkert halos suffer from the same distance problem as the NFW halo models: the sizes at the HIPASS sensitivity threshold are simply too small to allow them to be placed at distances much larger than $d \approx 200$ kpc from the Milky Way. Our results are in excellent agreement with those of Kepner, Babul & Spergel (1997) and Kepner *et al.* (1999), who calculated the chemical, thermal, and ionization equilibrium of gas in dark matter minihalos with Burkert density profiles. They found that the characteristic radius at the $N_{\text{HI}} \approx 10^{18} \text{ cm}^{-2}$ level never exceeded $r \approx 1$ kpc, even when the central hydrogen column density reached values much larger than any we consider here.

The combination of these two factors (the large mass that is required in order to have plausible gas to dark matter ratios for NFW halos, and the close distances required by the small physical size of the clouds for either NFW or Burkert halos) is fatal for any model in which the CHVCs represent a population of cosmological objects. In Figure 10 we show the halo mass distribution for a cosmological simulation of the Local Group (Moore *et al.* 2001). The ~ 2000 halos were created by analyzing the formation of a binary pair of massive halos in a hierarchical universe dominated by cold dark matter. The masses, separation and relative velocities of the binary halos are close to those observed for the Milky Way and Andromeda. The binary system was chosen from a large cosmological simulation such that a nearby massive cluster similar to Virgo was present. The simulation is described in detail in Moore *et al.* (2001). The filled circles show all of the halos (aside from those representing the Milky Way and Andromeda galaxies) within the simulated Local Group volume and the open circles show the halos that lie within 200 kpc of the Galaxy. As we showed above, the minimum acceptable mass for CHVC halos is $M_{dm} \sim 5 \times 10^8 M_\odot$. From this mass limit up to $M_{dm} = 2 \times 10^9 M_\odot$, there are 16 halos in the simulation⁶ To explain the CHVCs as cosmological, dark matter-dominated objects, we need approximately 250. Hence unless the hierarchical, cold dark matter-dominated cosmology grossly *under-predicts* the number of halos in this mass range, our results do not allow CHVCs to represent such a population.

4.3. CHVC HI distribution

There have now been several detailed studies of the HI structure of CHVCs. Wakker & Schwarz (1991) investigated two CHVCs and were the first to notice the core/halo structure of the clouds. Braun & Burton (2000) imaged six CHVCs at $1'$ resolution and found compact cores with linewidths as low as 2 - 10 km s^{-1} , as well as the large diffuse halo modeled here with linewidths of $\sim 25 \text{ km s}^{-1}$. The warm ($\sim 10^4 \text{ K}$) halos were imaged at $3'$ resolution with Arecibo by Burton, Braun &

⁶For a lower mass limit of $M_{dm} \sim 10^8 M_\odot$, as allowed for Burkert profile halos, the number of halos would be a few times larger. However, except for extreme assumed CHVC parameters (*i.e.*, peak column densities and linewidths much larger than the typical values), the CHVC models with Burkert halos will be physically even smaller than those with NFW halos. Hence these objects would have to lie closer than 200 kpc, and so the total number predicted would be about the same as for the NFW-halo models.

Chengalur (2001; hereafter BBC).⁷ They argued that the column density distribution at the edges of the clouds (for $N_{\text{HI}} < 10^{18.5} \text{ cm}^{-2}$) drops off as an exponential with radius, indicating a spherical exponential distribution of neutral hydrogen volume density as a function of radius. (Figures 11 and 12 of BBC demonstrate the quality of the exponential fits.) Kinematically the cores and halos of the CHVCs do not appear to be related. BBC derived distances of typically a few hundred kpc for the clouds in their sample, based on the following assumptions:

- The neutral gas density distribution is reasonably well-described by an exponential with radius, so that the central density can be inferred from the peak column density and the fit scalelength;
- The gas neutral fraction is close to unity in the center of the CHVC, and the temperature $T \sim 10^4$ K;
- The total gas pressure at the center is $P/k \sim 100 \text{ cm}^{-3} \text{ K}$, which Braun & Burton (2000) argued is the characteristic pressure at which the cold cores can co-exist with the warm neutral medium.

With these assumptions, the angular scale length of the exponential can be converted to a physical scale length, thereby yielding a cloud distance.

In this section we show that the characteristic exponential N_{HI} profile arises as a simple consequence of the physics of photoionization, and in the absence of fine-tuning of conditions, is very unlikely to provide reliable distance estimates.

In Figure 11 we plot the projected neutral hydrogen column density as a function of impact parameter (normalized to the cloud radius) for five different uniform density models, with total densities n_{H} between 10^{-4} and 10^{-2} cm^{-2} . For all of these models the N_{HI} profile resembles an exponential over most of the cloud radius, with the exception of a core which becomes more pronounced with increasing density, and of a cutoff as the cloud outer boundary is approached. The exponential appearance of the H I column density distribution indicates that the neutral hydrogen volume density distribution is also approximately an exponential, at least over a substantial fraction of the cloud volume. This is simply a consequence of the photoionization physics, and reflects the attenuation of the ionizing radiation (and therefore the increase in the neutral fraction) with depth into the clouds; the total gas volume densities in all these models are uniform.

⁷Of the ten CHVCs imaged by BBC at Arecibo, 8 are covered by the northern extension of the HIPASS survey. We have examined the HIPASS data for these clouds to see whether the HIPASS results have been seriously compromised by resolution effects. With the exception of the faintest cloud in the sample (for which the Arecibo peak column is about 4.5 times the HIPASS value: however, the column density peaks are due to probably unresolved, non-centered structure, and the entire western half of the cloud has a typical column extremely close to the HIPASS value), the Arecibo and HIPASS peak column densities differ by at most a factor of two. Hence there is no reason to think that the HIPASS observations systematically underestimate the cloud column densities significantly enough to affect the results of this paper.

BBC fit N_{HI} profiles of the form

$$N_{\text{HI}}(p) = 2n_o h \left(\frac{p}{h}\right) K_1(p/h) \quad (7)$$

to their observations, where p is the impact parameter, n_o is the central density, h is the scale-length, and K_1 is a modified Bessel function. This is the form expected for an exponential volume density distribution of infinite extent (van der Kruit & Searle 1981). This is modified for a cloud of finite extent, however, and so instead we use the finite-cloud profile

$$N_{\text{HI}}(p) = 2n_o h \left(\frac{p}{h}\right) \left[e^{-R/h} (R^2/p^2 - 1)^{1/2} + k_1(p/h, R/p) \right] \quad (8)$$

where R is the cloud radius and k_1 is an incomplete Bessel function,

$$k_1(\rho, x) = \rho \int_1^x e^{-\rho t} (t^2 - 1)^{1/2} dt \quad (9)$$

which goes to the usual $K_1(\rho)$ as $x \rightarrow \infty$.

In Figure 12 we show two examples of fits of equation (8) to the projected neutral hydrogen column density distributions for the CHVC models described in §4.1. These are not formal fits to the distributions, and are intended solely to show that these uniform density models are very well described over a large range in radius (in fact, everywhere except for the cores) by an exponential n_{HI} distribution. Although BBC argued based on observations of dwarf galaxies that there is a characteristic value of h , that conclusion does not hold for these models, as h depends nontrivially on the volume density. For the pair of models shown in Figure 12, which differ in n_{H} by a factor of two, the fitted values of h differ by nearly a factor of four.

The BBC distance method generally yields erroneous results when applied to these models, for two reasons: (1) many of the CHVC models have substantial ionized fractions even in their cores, so that the central neutral density - even if determined with reasonable accuracy from the exponential fit - can be substantially below the actual total gas density, and (2) the central pressure is generally not equal to $P/k \sim 100 \text{ cm}^{-3} \text{ K}$.⁸ It is not at all obvious that the value of $P/k \sim 100$ quoted by Braun & Burton (2000) for the co-existence of cold gas with the warm neutral medium is generally applicable. This conclusion was based on a phase diagram calculated by Wolfire *et al.* (priv. comm.) for “Local Group conditions”, which are not otherwise specified. In the calculations of Wolfire *et al.* (1995a,b), which presumably use similar physics, gas heating is dominated by grain photoelectric heating, and the only source of ionizing photons is the extragalactic soft X-ray background, which produces an ionizing flux about an order of magnitude smaller than assumed here. Furthermore, the resulting phase diagram is rather sensitive to the adopted gas parameters

⁸For the $n_{\text{H}} = 0.01 \text{ cm}^{-3}$ model, for which P/K does equal 100 at cloud center, the BBC distance method gives a result within about 25% of the value assigned to the cloud ($D = 67 \text{ kpc}$, Table 1) in order to make its angular size match the typical HIPASS size, provided that the true central column density is used, rather than the fitted column density, since in these relatively high-density models the presence of a core means that the exponential fit overestimates the central column density - *cf.* Figures 11 and 12.

(see Figures 1 and 6 in Wolfire *et al.* 1995b, in which the range of pressures over which a two-phase medium is allowed can extend over three orders of magnitude). In fact, in the phase diagram presented by Braun & Burton (their Figure 13), the minimum pressure P_{min} for which the cold phase exists is approximately five times larger ($P_{min}/k \approx 300 \text{ cm}^{-3} \text{ K}$) for a CHVC warm gas column density $N_{\text{HI}} = 10^{19} \text{ cm}^{-2}$, as appropriate for the HIPASS CHVCs discussed here, than it is for $N_{\text{HI}} = 10^{20} \text{ cm}^{-2}$ (for which P_{min}/k is actually about 60), as adopted by Braun & Burton for their sample. This would reduce the inferred distances by a factor of three. It is also not yet clearly established that the presence of cold gas is a generic property of CHVCs: there are only six clouds in the Braun & Burton (2000) sample, and while all of these exhibit cold cores, a much larger sample is clearly needed. The Magellanic Stream shows no evidence for cold gas (Mebold *et al.* 1991).

Interestingly, the models in which the gas is confined by a dark matter potential are not well described by profiles of the form (7) or (8). We show one such NFW model in Figure 13. This is the $M_{dm} = 5 \times 10^8 M_{\odot}$, no-core model shown as the solid line in the center panel of Figure 7. Inspection of that figure shows that the shape of the neutral hydrogen column density distribution in these dark matter-dominated models is generic. As is evident from Figure 13, these models cannot be described by a single component of the form (7) or (8). This is because the neutral hydrogen column density always exhibits a core with an extended wing, in consequence of the gas density profiles in these halos (*cf.* Figure 5). Hence the profile fit to the core of the N_{HI} distribution (we have used equation (7) for these models, since the models are actually much larger than the plotted region, and hence the cutoff is unimportant here), shown by the dashed line in Figure 13, grossly under-predicts N_{HI} outside $r \sim 0.5 \text{ kpc}$, while the fit to the column density distribution at larger radius (dotted line) falls an order of magnitude short of N_{HI} at $r = 0$. The results for Burkert profile halos are similar; in Figure 14 we show the neutral column density distribution for the largest column density model ($N_{\text{HI}}(0) = 1.0 \times 10^{20} \text{ cm}^{-2}$) shown in the lefthand panel of Figure 8 ($M_{dm} = 10^8 M_{\odot}$, $\sigma_g = 10.6 \text{ km s}^{-1}$). As for the NFW halo model, there is no reasonable fit with a single component of the form (7) or (8); in fact, the core-halo structure is even more pronounced than in the NFW halo. As before, fits to the core of the N_{HI} distribution (here we had to use equation [8]) severely underestimate N_{HI} beyond $r \sim 0.8 \text{ kpc}$, while fits to N_{HI} at large radius underestimate the column density at small radii by an order of magnitude.

5. Summary and Discussion

Models in which the compact high-velocity clouds (CHVCs) lie at distances of hundreds of kpc to $\sim 1 \text{ Mpc}$ from the Galaxy have such low volume densities of hydrogen that exposure to the extragalactic ionizing background radiation alone will largely ionize them. For models of uniform density clouds (§4.1), we find that the total hydrogen column needed to produce the typical neutral hydrogen column of $N_{\text{HI}} = 10^{19} \text{ cm}^{-2}$ ranges between 3 and 200 times N_{HI} (Figure 1) as the total hydrogen density varies between 10^{-2} and 10^{-4} cm^{-3} . The total gas masses of these clouds are therefore much larger than the apparent neutral gas masses. To match the typical angular size

seen for CHVCs in the HIPASS survey, low-density clouds must be at large distances and have correspondingly large masses. Models in which the cloud hydrogen densities are less than $n_{\text{H}} \approx 2 - 3 \times 10^{-3} \text{ cm}^{-3}$ are ruled out, as such clouds would have to lie outside the Local Group (*cf.* Figures 2 and 3).

At Local Group distances, $d \sim 0.7 - 1$ Mpc, the gas mass alone of the individual CHVCs would be $M_{\text{gas}} \sim 10^8 M_{\odot}$, and the mass of the observed population would be $M \sim 4 \times 10^{10} M_{\odot}$. Such CHVCs could have dark matter/gas mass ratios of only $\sim 2 - 3$ without producing line widths larger than the observed value. Models in which the CHVCs are at smaller distances, $d \sim 350$ kpc, with gas masses $M_{\text{gas}} \sim 10^7 M_{\odot}$, appear to be more reasonable, and could be dynamically compatible with plausible (~ 10 to 1) dark matter to gas mass ratios.

A closer examination of this scenario, however, using realistic dark matter halos, shows that it runs into severe difficulties (§4.2). This is because: (1) the sizes of the detectable H I clouds are too small ($R \lesssim 1$ kpc), which requires that the CHVCs are at distances $d \lesssim 200$ kpc (this is true whether we use NFW profiles or Burkert profiles for the halo dark matter density distribution); and (2) the halo masses required for reasonable ratios of $M_{\text{dm}}/M_{\text{gas}}$ for NFW halos are too large ($M_{\text{dm}} \sim 10^9 M_{\odot}$). Hence the predicted number of such objects in a hierarchical CDM structure formation scenario is more than an order of magnitude smaller than the observed number of CHVCs, and CHVCs cannot represent a population of infalling, cosmological objects.

We have also examined the suggestion that the approximately exponential N_{HI} profiles seen in high resolution studies of a sample of CHVCs could provide an estimate of the cloud distances (§4.3). Such profiles are a natural consequence of an external source of ionizing photons for clouds with uniform total density. The derived scale lengths are not constant and depend on the cloud density. We argue that this technique cannot be used to derive distances to the CHVCs in a model-independent way, as the scale lengths are not fixed and the alternative assumption of a constant pressure for the CHVC population is debatable. The CHVC N_{HI} profiles can be explained by photoionization even if the clouds are near to the Galaxy ($d \lesssim 100$ kpc).

Our models have assumed that the gas is smoothly distributed, and therefore do not include substantial clumping. This is arguably a plausible assumption for the CHVC envelopes that we have modeled in this paper, as the gas in these envelopes presumably is in the warm ($T \sim 10^4$ K, as is indicated by the observed linewidths) neutral phase, and is supported by the generally smooth distributions and reflection symmetry seen in high-resolution studies of the envelopes (BBC). The only way in which this assumption can be substantially in error, and the gas highly clumped, is if the clumps are in the cold neutral phase, with temperatures of order 100 K. In this case the observed linewidths must reflect bulk motion rather than thermal velocities. Since the (thermal) linewidths of individual clumps would be $\Delta V \sim 2 \text{ km s}^{-1}$, a large number of clumps would need to be present along any given sightline in order to explain the smoothness of the velocity profiles. Such clumps would also have to be substantially smaller than the spatial resolution of the high resolution imaging studies, which frequently do find (and resolve) small numbers of cores with narrow linewidths (*e.g.*, BBC). If pressures $P/k \sim 100 \text{ cm}^{-3} \text{ K}$ are necessary to drive the gas into the cold neutral phase (BBC), then the hydrogen densities must be at least $n_{\text{H}} \sim 1 \text{ cm}^{-3}$. It

is rather difficult to see how to make such a density structure compatible with the observations. If the clumps are self-gravitating, then they must have column densities that are much larger than the beam-averaged column densities measured observationally, which requires that the areal filling factor is small even though the filling factor in velocity space must be large to reproduce the observed line profiles. If they are not self-gravitating, we are left with the question of what confines them (or generates them, if they are transient objects). Hence we consider it unlikely that the CHVC envelopes that we have considered in this paper actually consist of dense, cold clumps rather than relatively smooth warm neutral gas.

What possibilities does this leave us with for the nature of CHVCs? Clouds without dark matter located within the confines of the Local Group are not massive enough to be self-gravitating, and must be either transient or confined by some external medium. Either of these scenarios would seem to argue for the CHVCs being associated with the Galaxy rather than the Local Group, as both the relatively short dynamical timescale ($t \sim 10^8$ years) and the presence of a confining medium are much more easily understood if the CHVCs are connected to the flux of mass and energy through the Galactic halo. This suggestion is supported by the overall similarities of the CHVCs to the remainder of the HVC population (Putman *et al.* 2002). The total and neutral hydrogen gas masses of the entire observed CHVC population (~ 250 objects) would be $M_{gas} \sim 7 \times 10^8 M_{\odot}$ and $M_{HI} \sim 7 \times 10^7 M_{\odot}$, respectively, at $d \approx 200$ kpc, and scale nearly as d^2 for smaller distances.

We are grateful to several colleagues, especially Nick Gnedin and Jessica Rosenberg, for helpful discussions. Nick kindly provided the software (written by Oleg Gnedin) for calculating the properties of NFW halos. PRM is supported by the National Science Foundation under grant AST 99-00871 and by NASA through HST grant AR-08747.02-A. MEP is supported by NASA through Hubble Fellowship grant HST-HF-01132.01-A awarded by the Space Telescope Science Institute, which is operated by the Association of Universities for Research in Astronomy, Inc., for NASA, under contract NAS 5-26555.

REFERENCES

- Barnes D., Staveley-Smith L., *et al.* 2001, MNRAS, 322, 486
- Blitz L., Spergel D., Teuben P., Hartmann D., & Burton W.B. 1999, ApJ, 514, 818
- Braun R. & Burton W.B., 1999, A&A, 341, 437
- Braun R. & Burton W.B. 2000, A&A, 354, 853
- Burton W.B., Braun R. & Chengalur J. 2001, A&A, 369, 616
- de Heij V., Braun R. & Burton W.B. 2002, A&A, 392, 417
- Haardt, F., & Madau, P. 1996, ApJ, 461, 20
- Kulkarni, V.P., & Fall, S.M. 1993, ApJ, 413, L63

- Madsen, G.J., Reynolds, R.J., Haffner, L.M., Tufte, S.L., & Maloney, P.R. 2001, ApJ, 560, L135
- Maloney P., 1993, ApJ, 414, 41
- Maloney, P.R., & Bland-Hawthorn, J. 1999, in Stromlo Workshop on High-Velocity Clouds, ed. B.K. Gibson & M.E. Putnam (San Francisco: Astronomical Society of the Pacific), 199
- Mebold, U., Herbstmeier, U., Kalberla, P.M.W., Greisen, E.W., Wilson, W., & Haynes, R.F. 1991, A&A, 251, L1
- Moore, B., Calcáneo-Roldán, C., Stadel, J., Quinn, T., Lake, G., Sebastiano, G., & Governato, F. 2001, PhysRevD, 64, 063508
- Mohr, J.J., Mathiesen, B., & Evrard, A.E. 1999, ApJ, 517, 627
- Oort, J.H., 1966, Bull. Astron. Inst. Netherlands, 18, 421
- Putman M.E., *et al.*, 2002, AJ, 123, 873
- Scott, J., Bechtold, J., Morita, M., Dobrzycki, A., & Kulkarni, V.P. 2002, ApJ, in press.
- Shull, J.M., Roberts, D., Giroux, M.L., Penton, S.V., & Fardal, M.A. 1999, AJ, 118, 1450
- van der Kruit, P.C., & Searle, L. 1981, A&A, 95, 105
- van Gorkom, J.H. 1993, in The Environment and Evolution of Galaxies, ed. J.M. Shull & H.A. Thronson (Dordrecht: Kluwer), 343
- Verschuur, G.L. 1969, ApJ, 156, 771
- Wakker, B.P. & Schwarz, U. 1991, A&A, 250, 484
- Weymann, R.J., Vogel, S.N., Veilleux, S., & Epps, H. 2001, ApJ, 561, 559
- Wolfire, M.G., Hollenbach, D., McKee, C.F., Tielens, A.G.G.M., & Bakes, E.L.O. 1995a, ApJ, 443, 152
- Wolfire, M.G., McKee, C.F., Hollenbach, D., & Tielens, A.G.G.M. 1995b, ApJ, 453, 673

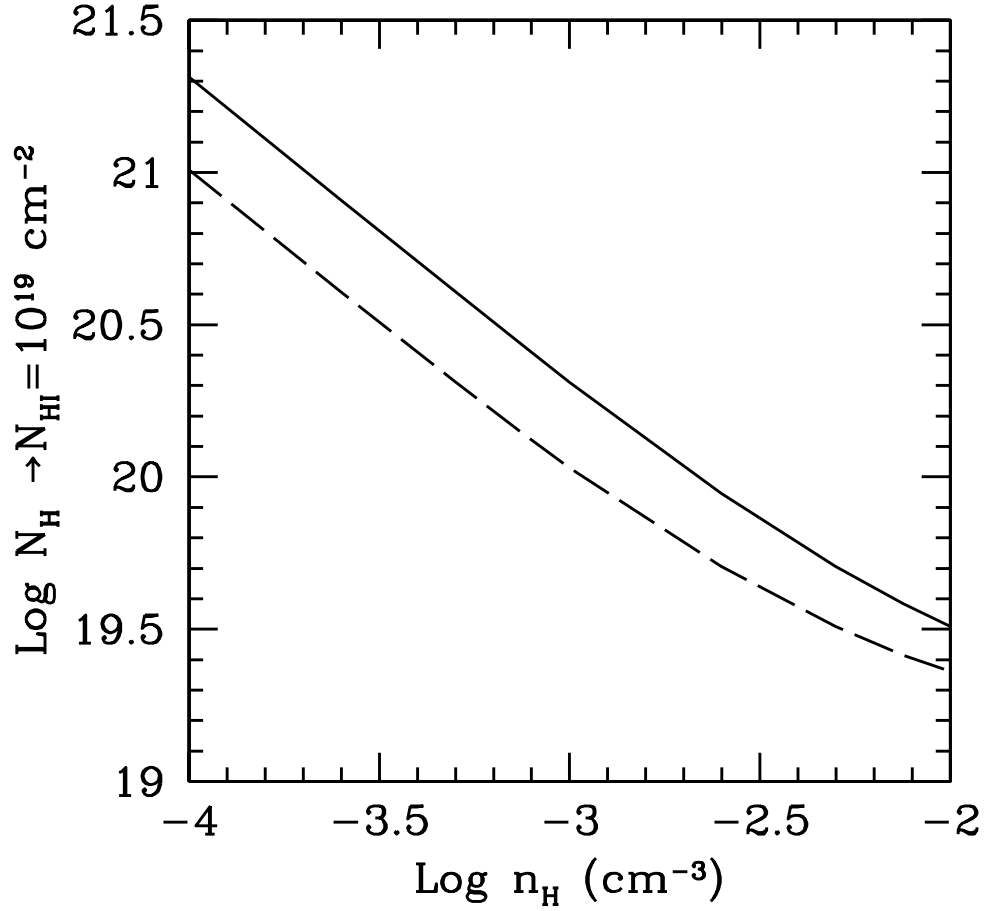


Fig. 1.— The total hydrogen column density N_H required to obtain a neutral hydrogen column density $N_{\text{HI}}=10^{19} \text{ cm}^{-2}$, as a function of the total hydrogen density. The solid curve is for an ionizing flux $\phi \sim 10^4 \text{ phot cm}^{-2} \text{ s}^{-1}$; the dashed curve shows the effect of reducing ϕ by a factor of two. In the latter case the values of N_H are smaller by a factor of two at the low-density end compared to the fiducial model.

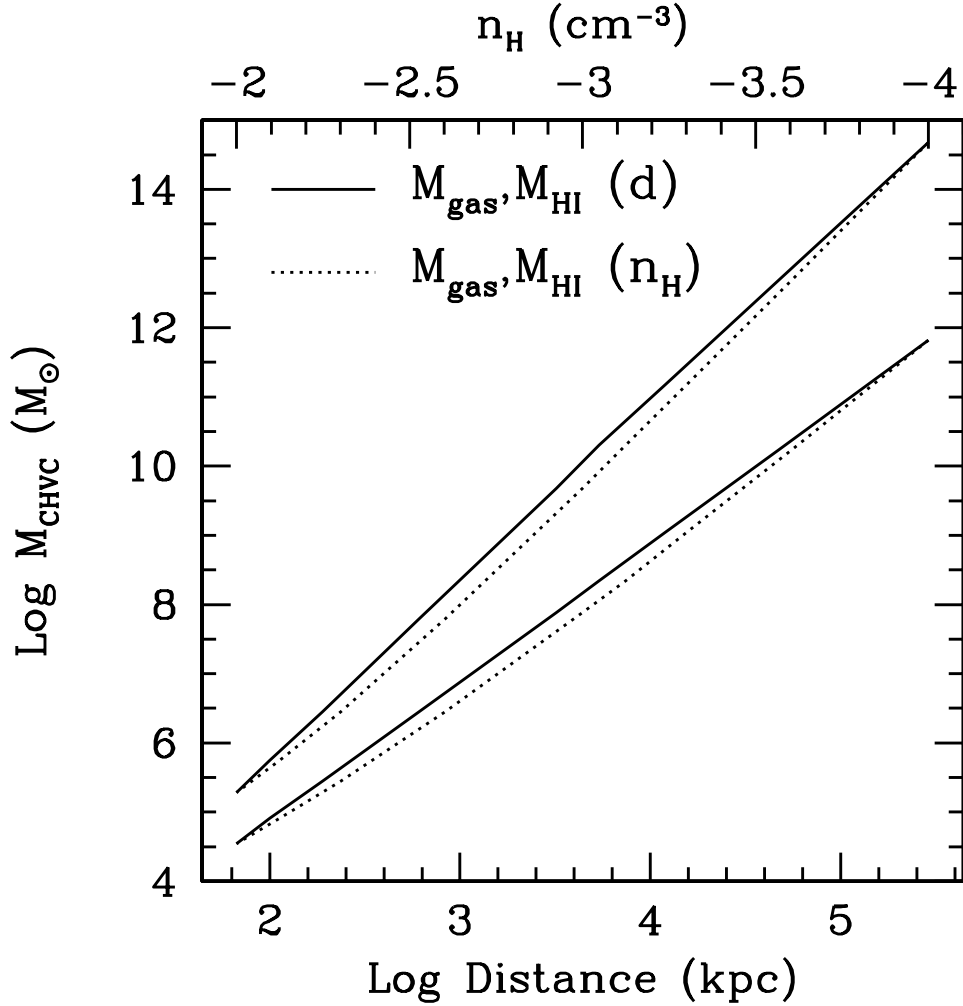


Fig. 2.— The total (neutral plus ionized) and apparent (derived from the neutral column density and apparent size) gas masses, plotted vs. distance and total H density. For each model (*i.e.*, assumed total hydrogen density), the distance d is determined from the requirement that the apparent angular size (determined using the radius for which the projected neutral hydrogen column drops to the HIPASS sensitivity limit, $N_{\text{HI}} = 2 \times 10^{18} \text{ cm}^{-2}$) matches the typical size seen in the HIPASS sample of CHVCs, for which the angular radius $\Delta\theta \sim 0.34$ degrees. The masses as a function of density (top axis) are plotted as dashed lines, and as a function of distance (bottom axis) as solid lines; the true gas mass M_{gas} is always greater than the apparent mass M_{HI} .

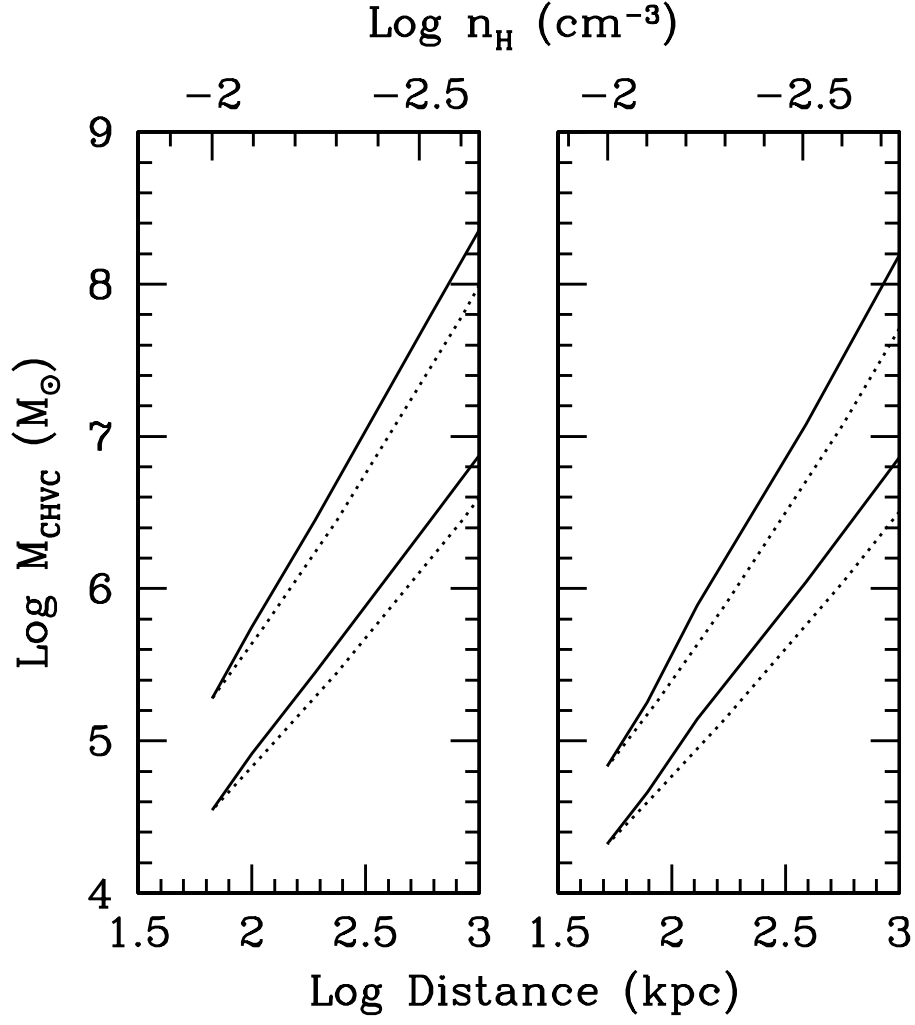


Fig. 3.— The total and apparent gas masses, plotted vs. distance and total H density, as in Figure 2. The left panel shows the results for our fiducial ionizing flux $\phi_i \sim 10^4$; the right panel is for ϕ_i reduced by a factor of two.

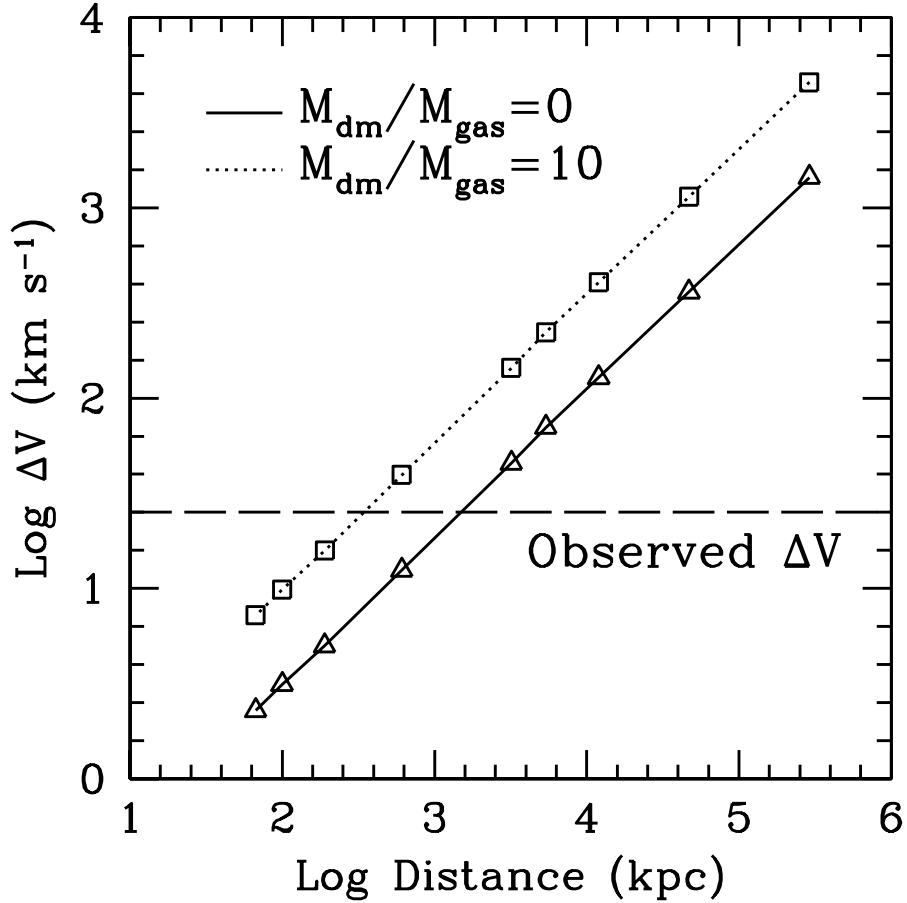


Fig. 4.— Predicted line FWHM vs. distance, for dark matter to gas mass ratios of 10 and 0, for the model CHVCs. As in Figure 2, the distance is determined by requiring that the apparent angular size equals the typical CHVC angular size seen in the HIPASS survey. The observed line width, $\Delta V \sim 25 \text{ km s}^{-1}$, is shown as the long-dashed line. The models are consistent at $d \sim 330 \text{ kpc}$ with $M_{dm}/M_{gas} = 10$ (dotted line) and at 1.5 Mpc with no dark matter (solid line). For the reduced ϕ_i models (not shown), the intercepts are at $d \sim 430 \text{ kpc}$ and $d \sim 2.1 \text{ Mpc}$ for 10:1 and no dark matter, respectively.

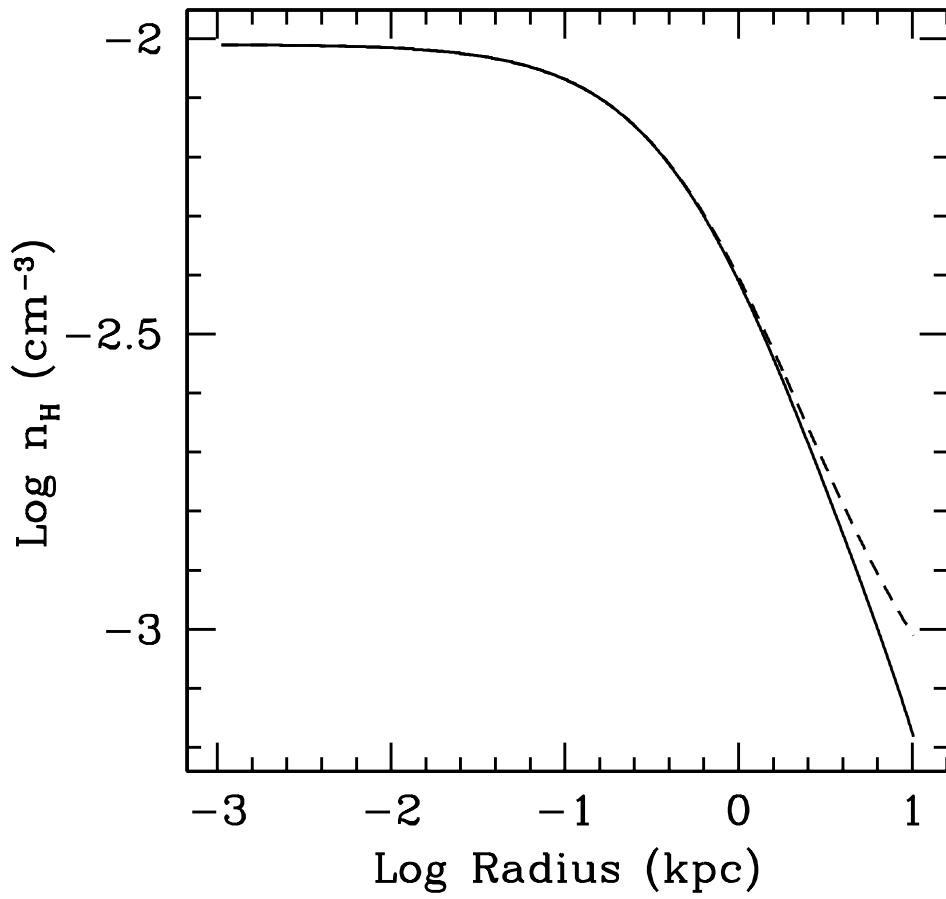


Fig. 5.— The gas density distribution in a NFW dark matter halo of mass $M_{dm} = 1.4 \times 10^8 M_{\odot}$ (solid line); the dashed line shows the density profile in the limit of negligible gas self-gravity.

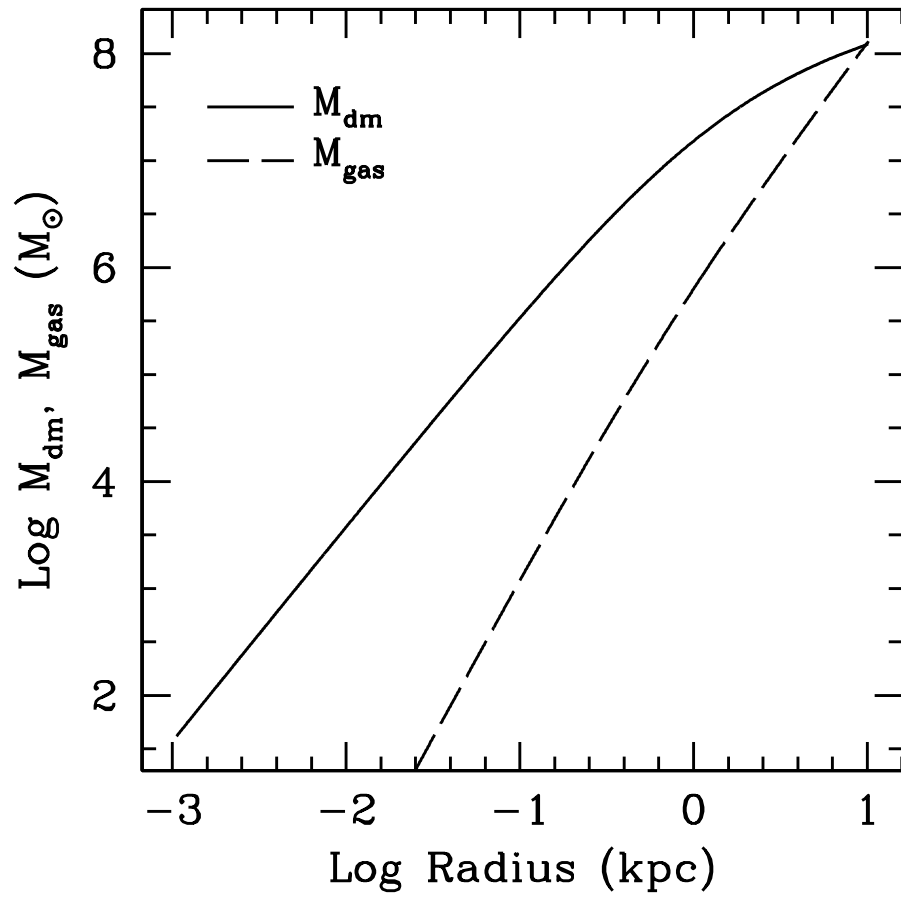


Fig. 6.— The cumulative dark matter and gas masses for the halo shown in Figure 5. The ratio $M_{gas}/M_{dm} \approx 1$ for this model.

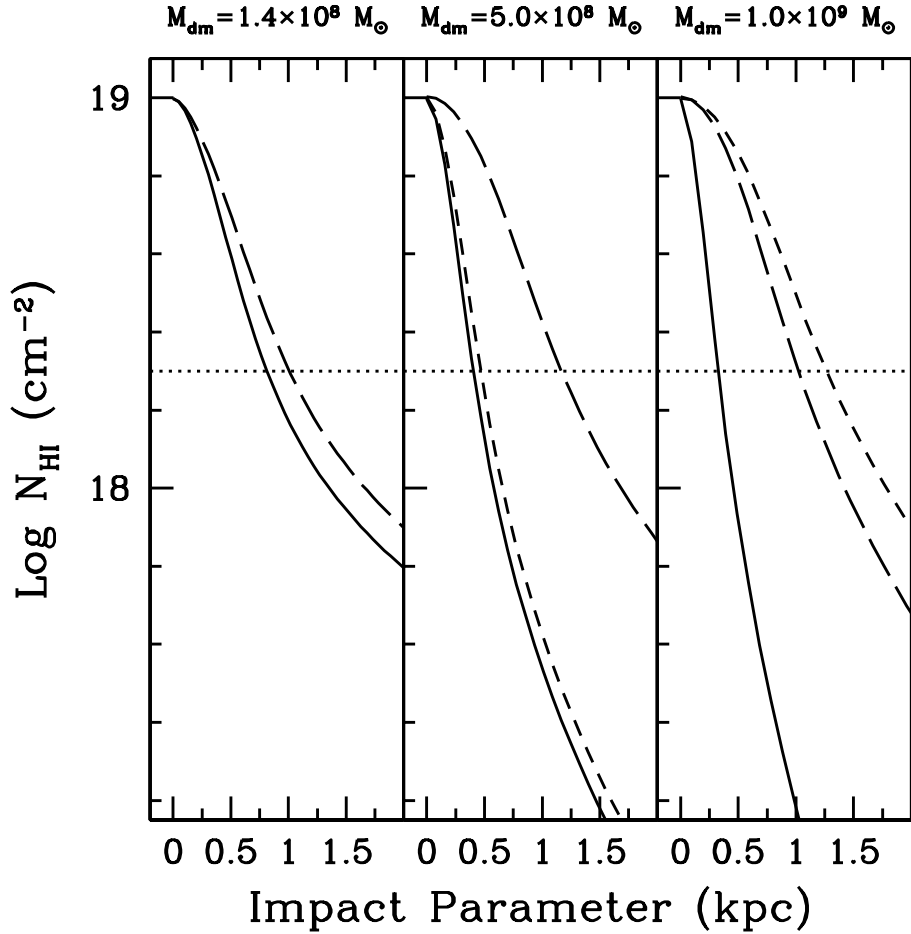


Fig. 7.— The projected neutral hydrogen column as a function of impact parameter, for several different NFW halo models. From left to right, the panels are for halo dark matter masses $M_{dm} = 1.4 \times 10^8 M_{\odot}$, $5.0 \times 10^8 M_{\odot}$, and $1.0 \times 10^9 M_{\odot}$, respectively. The dotted line running across the panels shows the HIPASS column density threshold of $N_{\text{HI}} = 2 \times 10^{18} \text{ cm}^{-2}$. Several models are shown in each panel. In the lefthand panel ($M_{dm} = 1.4 \times 10^8 M_{\odot}$), the solid curve is for our fiducial ionizing flux ϕ_o , and the long-dashed curve is for $\phi_i = \phi_o/2$. In the center panel ($M_{dm} = 5.0 \times 10^8 M_{\odot}$), the solid line is for $\phi_i = \phi_o$, the short-dashed line is for $\phi_i = \phi_o/2$, and the long-dashed line is for $\phi_i = \phi_o$ and a halo core radius $r_o = r_s$. In the righthand panel ($M_{dm} = 1.0 \times 10^9 M_{\odot}$), all models have $\phi_i = \phi_o$, and the solid, long-dashed, and short-dashed lines are for $r_o = 0$, r_s , and $2r_s$, respectively.

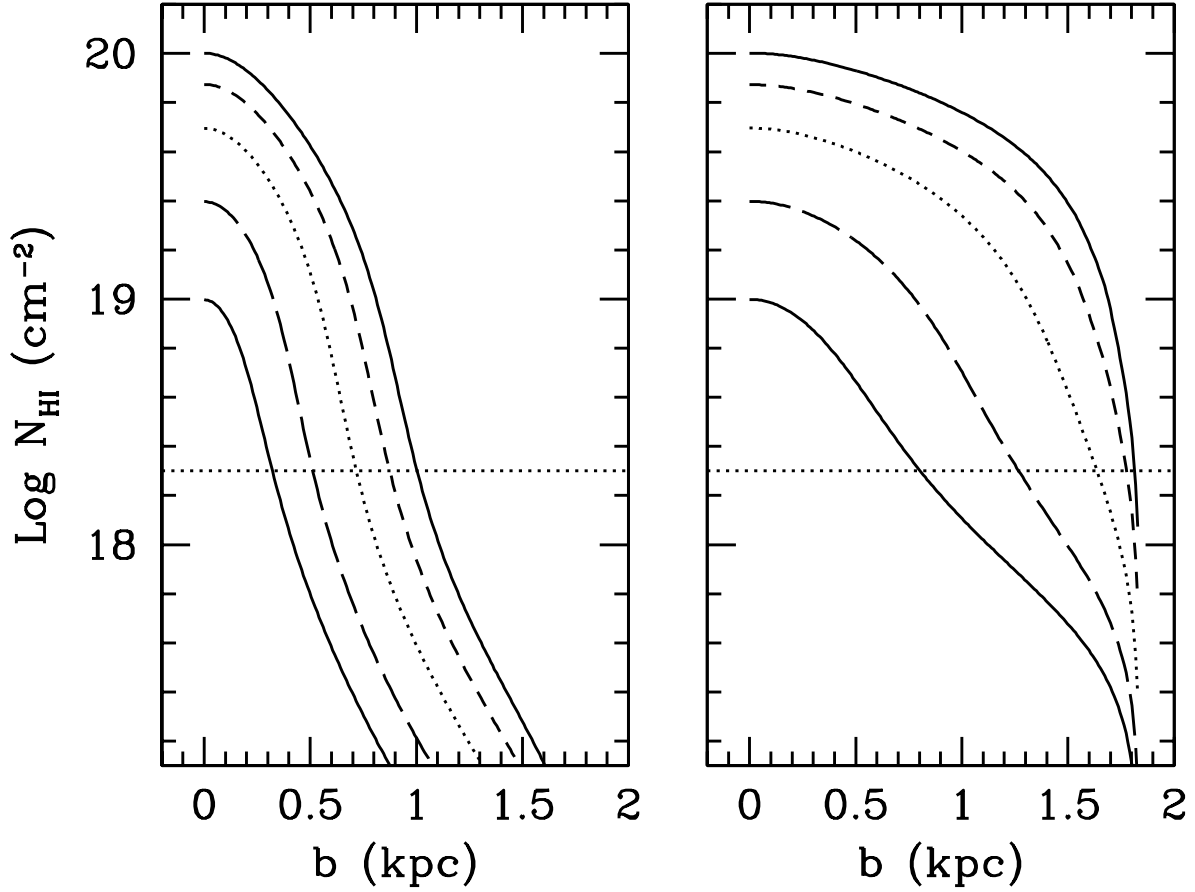


Fig. 8.— The projected neutral hydrogen column as a function of impact parameter, for Burkert halo models. The halo mass is $M_{dm} = 1.0 \times 10^8 M_{\odot}$. From left to right, the curves are for central neutral hydrogen column densities $N_{\text{HI}}(0) = 1.0 \times 10^{19}$, 2.5×10^{19} , 5.0×10^{19} , 7.5×10^{19} , and $1.0 \times 10^{20} \text{ cm}^{-2}$, respectively. In the lefthand panel a velocity dispersion of $\sigma_g = 10.6 \text{ km s}^{-1}$ has been assumed, while in the righthand panel $\sigma_g = 21.2 \text{ km s}^{-1}$. The dotted line running across the panels shows the HIPASS column density threshold of $N_{\text{HI}} = 2 \times 10^{18} \text{ cm}^{-2}$.

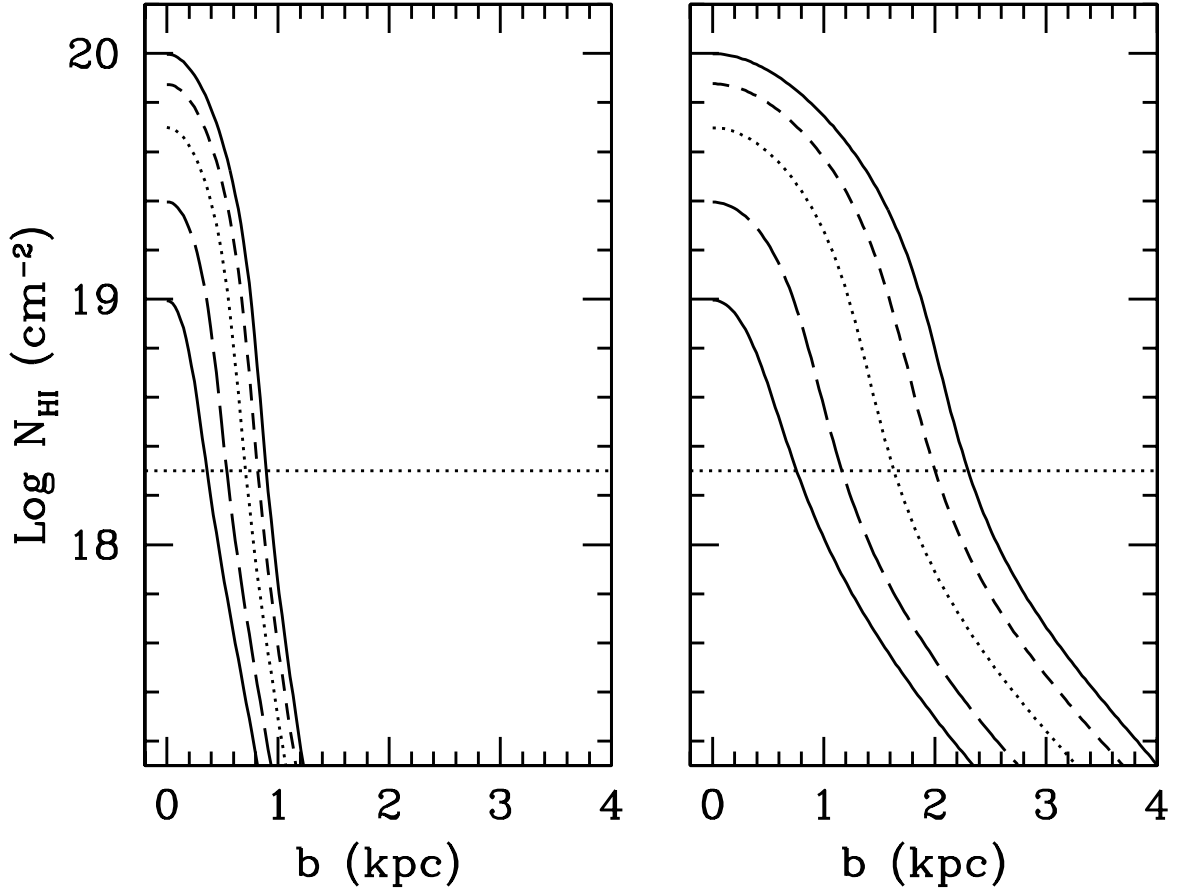


Fig. 9.— The projected neutral hydrogen column as a function of impact parameter, for Burkert halo models. The halo mass is $M_{dm} = 1.0 \times 10^9 M_{\odot}$. From left to right, the curves are for central neutral hydrogen column densities $N_{\text{HI}}(0) = 1.0 \times 10^{19}$, 2.5×10^{19} , 5.0×10^{19} , 7.5×10^{19} , and $1.0 \times 10^{20} \text{ cm}^{-2}$, respectively. In the lefthand panel a velocity dispersion of $\sigma_g = 10.6 \text{ km s}^{-1}$ has been assumed, while in the righthand panel $\sigma_g = 21.2 \text{ km s}^{-1}$. The dotted line running across the panels shows the HIPASS column density threshold of $N_{\text{HI}} = 2 \times 10^{18} \text{ cm}^{-2}$.

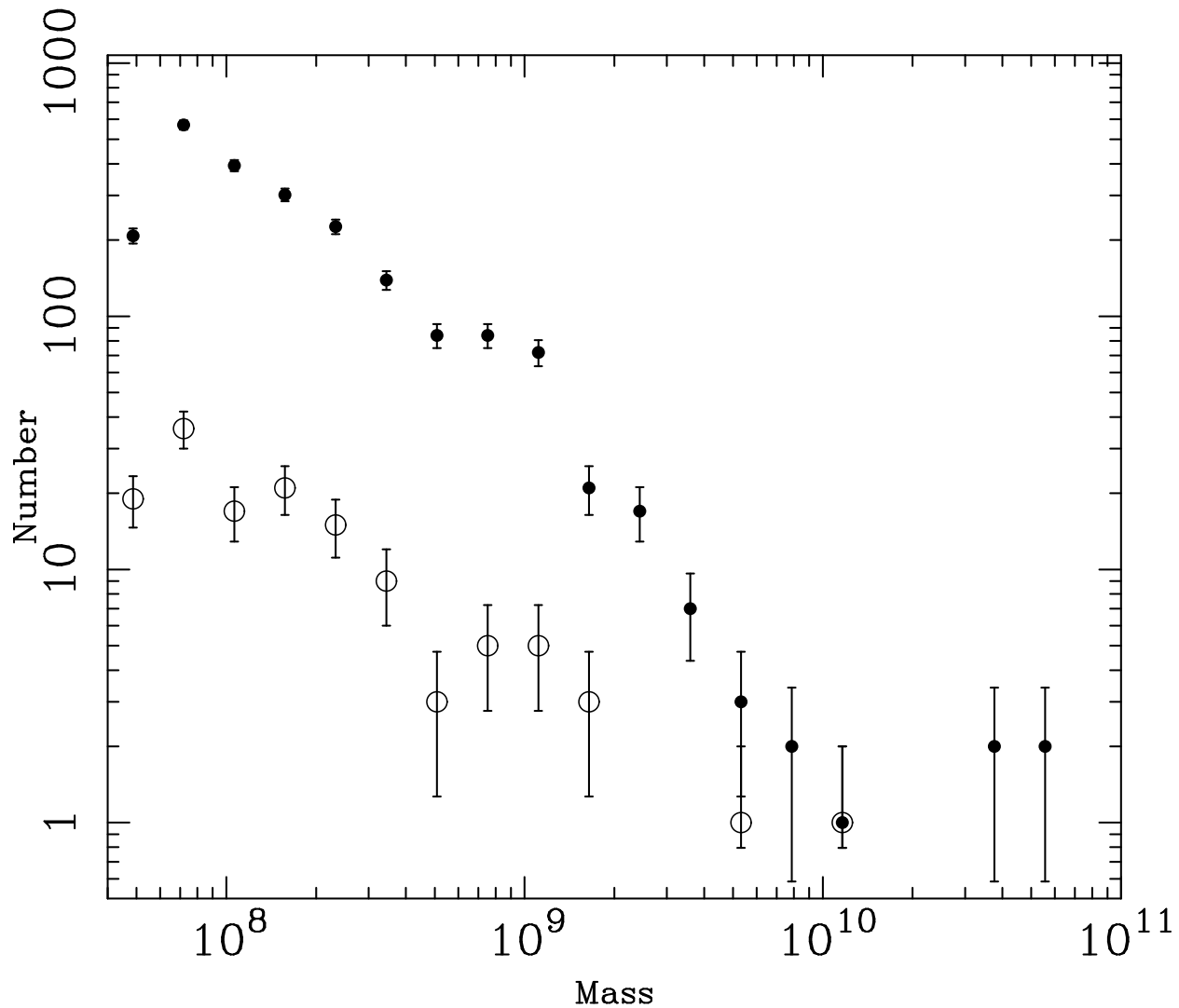


Fig. 10.— The halo mass distribution for a realization of the Local Group in a cold dark matter-dominated cosmological simulation. The filled circles show all of the halos (other than those representing the Milky Way and Andromeda) within the Local Group, and the open circles show all those that lie within 200 kpc of the Milky Way.

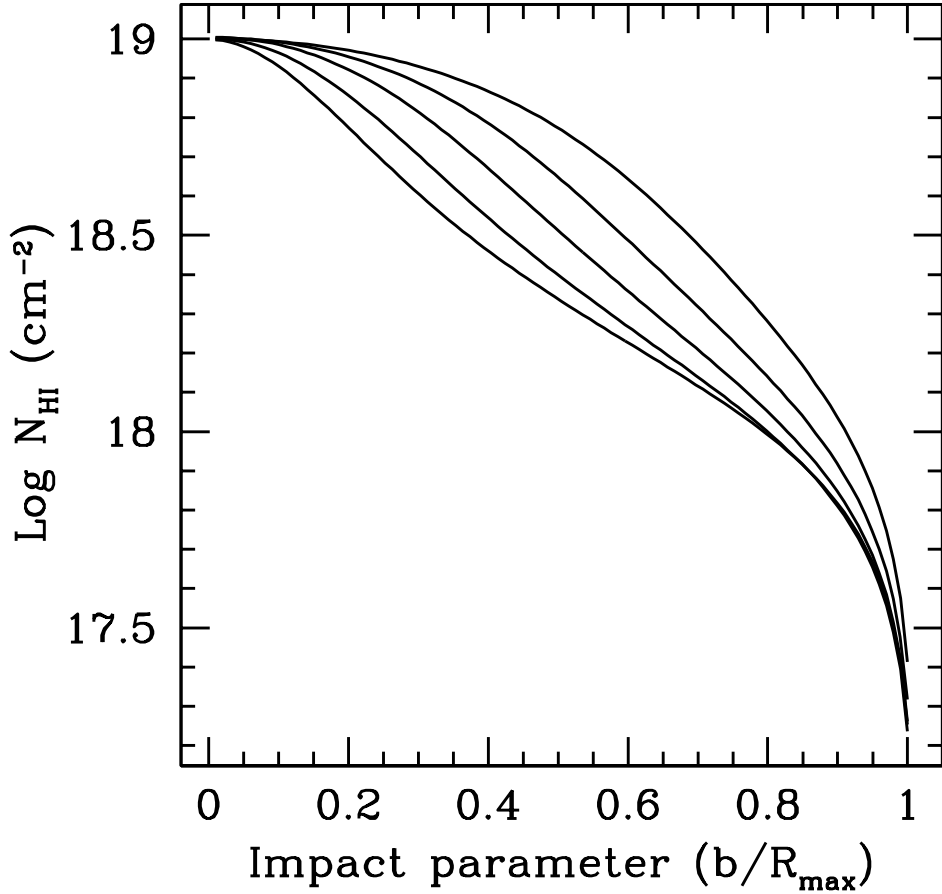


Fig. 11.— The neutral hydrogen column density as a function of normalized impact parameter (*i.e.*, the radial offset divided by the cloud radius) for different values of total hydrogen density. From top to bottom, the curves are for $n_{\text{H}} = 1.0 \times 10^{-2}$, 5.0×10^{-3} , 2.5×10^{-3} , 1.0×10^{-3} , and $1.0 \times 10^{-4} \text{ cm}^{-3}$. The profiles generally resemble exponentials except for the presence of a core, which becomes more prominent as the density is increased. The profiles also show a cutoff close to the outer boundary, but the latter occurs at neutral hydrogen columns below the detection threshold of the HIPASS survey.

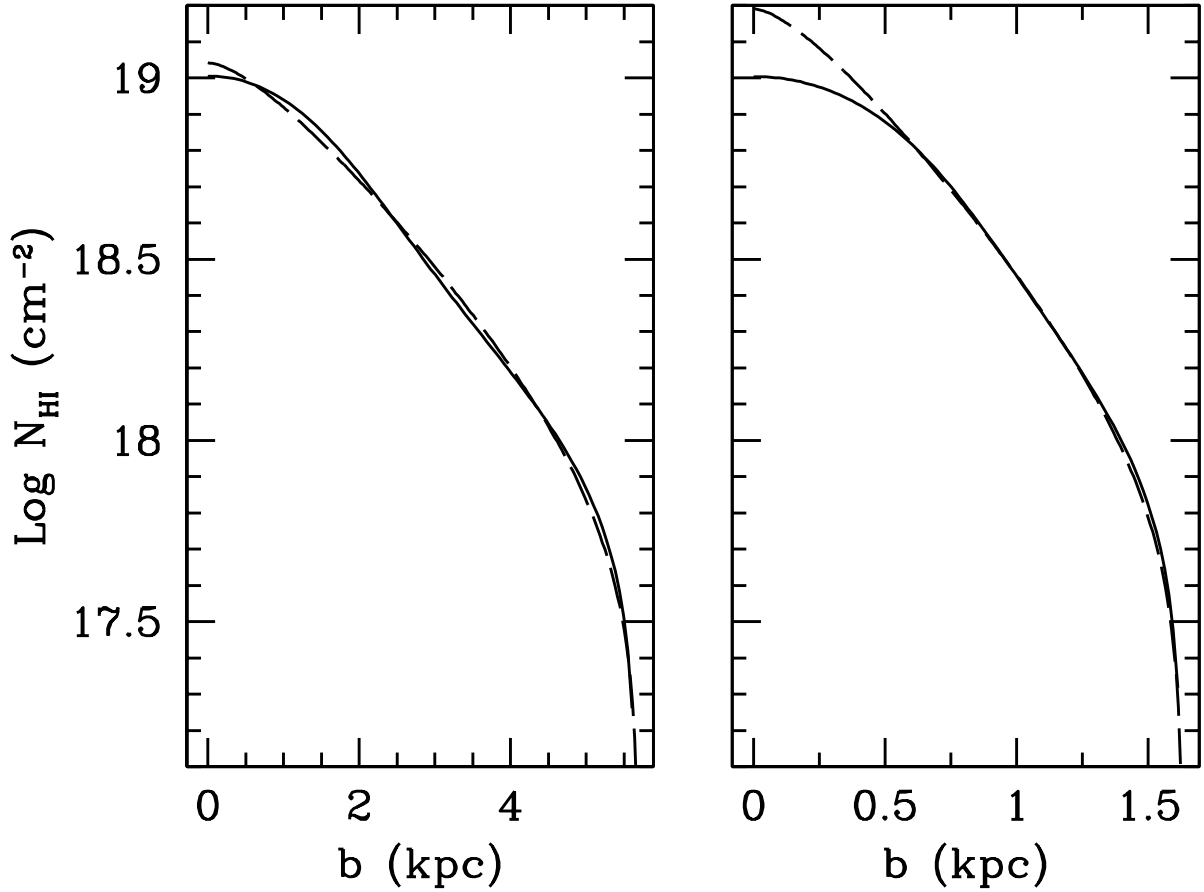


Fig. 12.— The neutral hydrogen column density (solid lines) as a function of impact parameter b for uniform density clouds with $n_{\text{H}} = 2.5 \times 10^{-3}$ (left panel), and 5.0×10^{-3} cm^{-3} (right panel). Also plotted are fits for projected exponential volume density distributions of neutral hydrogen, as discussed in the text (dashed lines). In both cases the cloud radius is identical to the maximum impact parameter. For the lefthand panel, the scale length $h = 1.5$ kpc and the central column density $N_{\text{HI}}(0) = 1.1 \times 10^{19}$ cm^{-2} , while for the righthand panel $h = 0.42$ kpc, $N_{\text{HI}}(0) = 1.55 \times 10^{19}$ cm^{-2} .

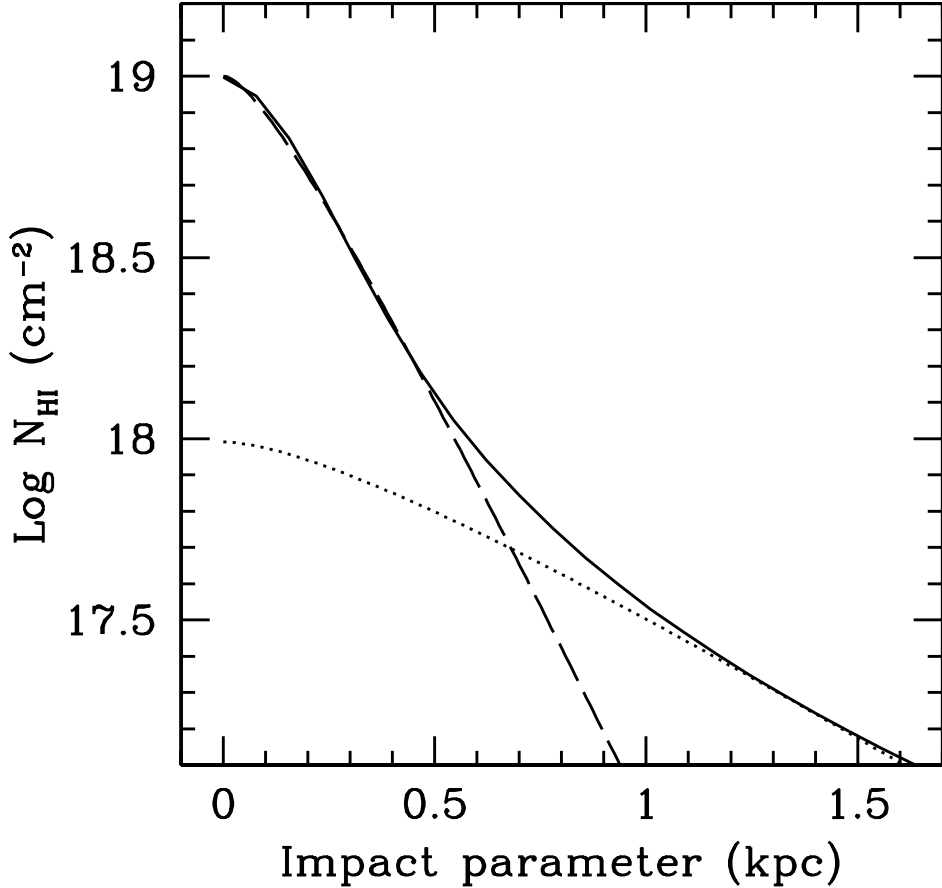


Fig. 13.— The neutral hydrogen column density (solid lines) as a function of impact parameter b for a CHVC model in which the gas is confined by a dark matter halo with a NFW profile. This halo has a mass $M_{dm} = 5 \times 10^8 M_{\odot}$, and is shown as the solid line in the center panel of Figure 7. Also plotted are fits for projected exponential volume density distributions of neutral hydrogen, as discussed in the text (dashed and dotted lines). The N_{HI} distribution cannot be fit by a single profile as given by equation (7) or (8). The inner and outer regions of the column density profile are fit by infinite gas distributions (equation [7]) with $h = 0.17$ kpc and central column density $N_{\text{HI}}(0) = 1.0 \times 10^{19} \text{ cm}^{-2}$ (dashed line) and $h = 0.55$ kpc, $N_{\text{HI}}(0) = 9.8 \times 10^{17} \text{ cm}^{-2}$ (dotted line), respectively.

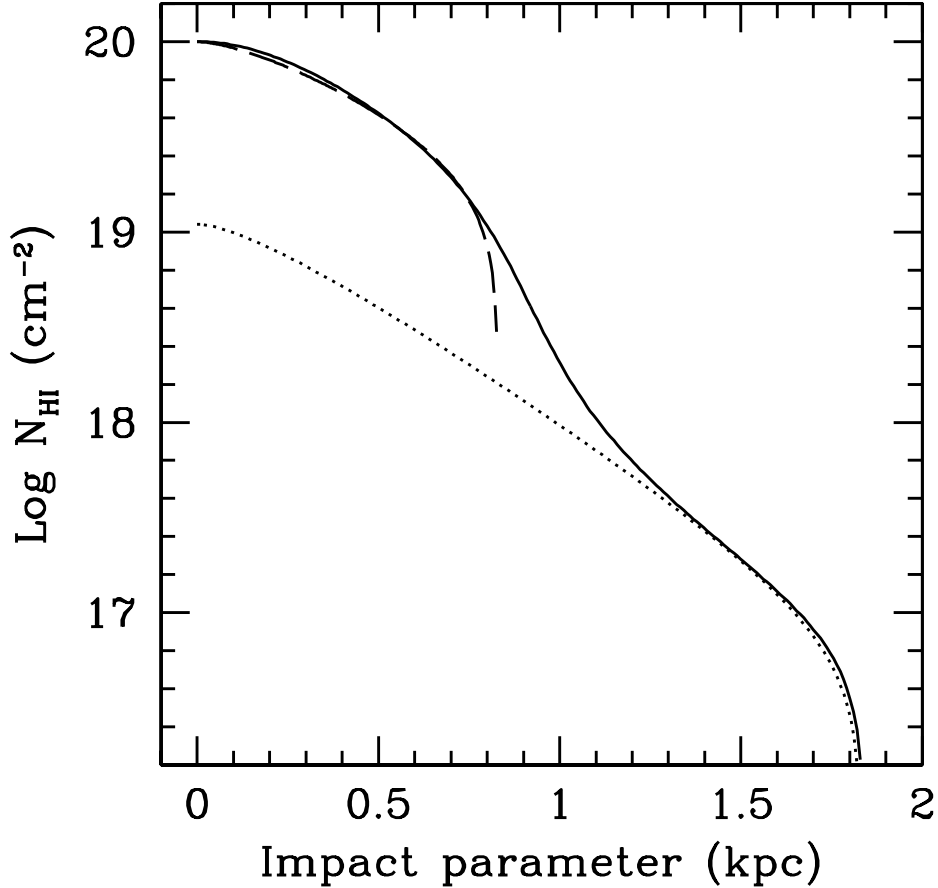


Fig. 14.— The neutral hydrogen column density (solid lines) as a function of impact parameter b for a CHVC model in which the gas is confined by a dark matter halo with a Burkert density profile. This halo has a mass $M_{dm} = 10^8 M_{\odot}$, and is shown as the rightmost solid line in the lefthand panel of Figure 8. Also plotted are fits for projected exponential volume density distributions of neutral hydrogen, as discussed in the text (dashed and dotted lines). The N_{HI} distribution cannot be fit by a single profile as given by equation (7) or (8). The inner and outer regions of the column density profile are fit by finite gas distributions (equation [8]) with $h = 0.4$ kpc and central column density $N_{\text{HI}}(0) = 10^{20} \text{ cm}^{-2}$ (dashed line) and $h = 0.3$ kpc, $N_{\text{HI}}(0) = 1.1 \times 10^{19} \text{ cm}^{-2}$ (dotted line), respectively. The cutoff radii for the two components are 0.83 kpc and 1.83 kpc, respectively.

Table 1: Results of CHVC models for an ionizing photon flux $\phi_i \sim 10^4 \text{ phot cm}^{-2} \text{ s}^{-1}$.^a

n_H (10^{-3} cm^{-3})	N_H (10^{19} cm^{-2})	r_H (kpc)	r_{HI} (kpc)	n_{HI} (10^{-3} cm^{-3})	D (kpc)	M_{HI} ($10^6 M_{\text{odot}}$)	M_{gas} ($10^6 M_{\text{odot}}$)	$M_{\text{dm}}/M_{\text{gas}}$
0.25	81.61	524	278	0.0058	47000	17000	4800000	–
0.50	40.60	130	71	0.023	12000	1100	150000	–
0.75	27.17	58	32	0.051	5400	220	20000	–
1.0	20.50	33	18.7	0.087	3200	76	4800	–
2.5	8.829	5.7	3.6	0.45	610	2.8	62	4
5.0	5.074	1.6	1.14	1.4	190	0.28	2.8	25
7.5	3.834	0.82	0.61	2.7	100	0.082	0.56	64
10.0	3.227	0.52	0.40	4.1	67	0.035	0.19	120

^aThe columns give the volume density of total hydrogen (n_H), the total hydrogen column (N_H) needed to produce a neutral column density of 10^{19} , the cloud radius (r_H), the radius at the HIPASS sensitivity limit (r_{HI}), the mean neutral hydrogen volume density (n_{HI}), the distance (D) required to match the typical HIPASS angular size, the apparent mass that would be derived from HI observations (M_{HI}), the total gas mass (M_{gas}), and the ratio of dark matter to gas mass needed to produce the typical observed line width of 25 km s^{-1} for *gravitational* confinement of the gas. (No entries are given for the $n_H \leq 10^{-3} \text{ cm}^{-3}$ models, as they violate the line width constraint with no dark matter.)